Pattern formation in slot-die coating ⏺FREE

Special Collection: Paint and Coating Physics

Maren Kasischke ⓘD ; Simon Hartmann ✉ ⓘD ; Kevin Niermann; Marco Smarra ⓘD ; Denis Kostyrin;
Uwe Thiele ⓘD ; Evgeny L. Gurevich ⓘD

Check for updates

CrossMark

View Online

Export Citation

Pattern formation in slot-die coating ⓔⓟ

🌐　　　⬆️　　　🔴
View Online　Export Citation　CrossMark

Maren Kasischke,[1] ⓘⅅ Simon Hartmann,[2,3,a] ⓘⅅ Kevin Niermann,[1] Marco Smarra,[1] ⓘⅅ Denis Kostyrin,[1] Uwe Thiele,[2,3,b]
ⓘⅅ and Evgeny L. Gurevich[1,4,c] ⓘⅅ

AFFILIATIONS

[1]Chair of Applied Laser Technology, Ruhr-Universität Bochum, Universitätsstraße 150, 44801 Bochum, Germany
[2]Institut für Theoretische Physik, Westfälische Wilhelms-Universität Münster, Wilhelm-Klemm-Str. 9, 48149 Münster, Germany
[3]Center for Nonlinear Science (CeNoS), Westfälische Wilhelms-Universität Münster, Corrensstr. 2, 48149 Münster, Germany
[4]Laser Center (LFM), University of Applied Sciences Münster, Stegerwaldstraße 39, 48565 Steinfurt, Germany

Note: This paper is part of the special topic, Paint and Coating Physics.
[a]Author to whom correspondence should be addressed: s.hartmann@wwu.de
[b]Electronic mail: u.thiele@uni-muenster.de
[c]Electronic mail: gurevich@lat.rub.de

ABSTRACT

We experimentally study the occurrence of pattern formation during the slot-die coating of partially wetting liquids onto polyethylenterephthalat-substrates outside the coating window. The experimental investigation is supported by numerical simulations of a dynamical model. Our results demonstrate that beyond a critical coating speed, the deposition of homogeneous coating layers undergoes an instability resulting in the self-organized emergence of patterned coatings, i.e., stripes of different orientation and droplet patterns. We investigate the transitions between the different patterns as triggered by changes in the control parameters inherent to slot-die coating, e.g., the liquid viscosity and the coating gap height. The relatively simple theoretical approach is based on lubrication theory. It is already able to reproduce most of the patterns observed experimentally and reveals a wettability-driven instability mechanism.

Published under an exclusive license by AIP Publishing. https://doi.org/10.1063/5.0150340

I. INTRODUCTION

The coating of flexible substrates with thin homogeneous layers is an important technological process relevant for many areas of modern life and various fields of technology, such as, e.g., analog photography, surface chemistry,[1] flexible electronics,[2,3] hydrogen fuel cells,[4,5] and organic photovoltaics.[6–10] Driven by technological needs, scientific investigations of the coating process, e.g., for slot-die or blade coating, are usually focused on specifying the *coating window*, i.e., the range of process parameters where a *homogeneous* defect-free coating of constant thickness is reproducibly achieved.[11–13] Depending on fluid and substrate properties as well as process parameters, outside this range instabilities occur that result in coating defects and patterned coatings.[14,15] The observed patterns include stripes parallel and orthogonal to the coating direction similar to patterns observed in other deposition processes,[16,17] including dip coating,[18–20] Langmuir–Blodgett transfer of surfactant layers onto a moving plate[21–23] and evaporative dewetting (aka "coffee-ring effect"), where a three-phase contact line driven by evaporation recedes on a solid substrate.[24–27] The focus of the present work is an analysis of the various occurring patterns and the corresponding transitions for the slot-die coating of a smooth solid substrate by a partially wetting liquid.

Sometimes, e.g., in the production of organic solar cells, initial coating steps that produce uniform deposited layers are followed by subsequent technological steps producing periodic patterns. This is, e.g., achieved by laser ablation of the layers.[28] Such post-processing patterning steps could be omitted if direct patterning by coating can be controlled in a similar way as control of patterning by Langmuir–Blodgett transfer and evaporative dewetting is used in applications.[29–31] A prerequisite is a detailed investigation and understanding of the nonequilibrium pattern formation that occurs outside the coating window. Here, we investigate the transition from homogeneous to patterned coating and the characteristics of the patterning process in dependence of the most important control parameters for slot-die coating of partially wetting low-viscosity, nearly Newtonian liquids onto polyethylenterephthalat (PET)-substrates. The focus is on slot-die coating as, similar to the closely related blade coating, it allows for rapid processing of large surface areas at standard atmospheric conditions, i.e., it can be incorporated into roll-to-roll processing.

The self-organized patterns emerging during coating are usually treated as unwelcome defects and are, therefore, barely studied in the literature. Normally, experimental investigations that consider the onset of coating instabilities, do not focus on the resulting pattern

25 July 2023 13:26:17

formation. Bhamidipati et al.[14] study patterning in slot-die coating induced by air entrainment in viscous non-Newtonian fluids. They observe the formation of periodic stripes and regular arrangements of bubbles in shear-thinning, non-Newtonian liquids with relatively high viscosity. Raupp et al.[15] observe the breakup of a homogeneous film and the formation of parallel stripes in a certain range of low film thicknesses and coating velocities, i.e., the velocity of the slot-die with respect to the surface to be coated. In both cases, the orientation of the stripes is parallel to the coating direction, i.e., the direction of slot-die movement. In other words, the stripes are perpendicular to the slot in the coating device. These parallel stripes separated by empty lanes are often referred to as "rivulets," while the occurrence of a continuous film that exhibits a weak transversal thickness modulation is referred to as "ribbing."[12,32] Some authors also use the term ribbing to describe rivulets.[15,33–35]

The ranges of Capillary numbers and of the distance between slot-die and substrate (gap height) that correspond to the coating window are also investigated for shear-thinning liquids,[36] where stripes oriented parallel ("barring") and perpendicular to the coating direction are observed. Mixed patterns are also possible. A review of operating limits in slot-die coating is given by Ding et al.,[13] where the numerous defects are related to several instability mechanisms of the upstream and downstream menisci. An instability of the downstream meniscus is usually attributed to the "low-flow limit," i.e., when the liquid fails to bridge the coating gap due to a strong curvature of the liquid profile at the downstream side, resulting in rivulets or ribbing.[11–13,15,37,38] Instability mechanisms of the upstream meniscus include the "high- and low-vacuum limits," which result from an imbalance between the air pressures at the upstream and downstream sides,[13] and the dynamic wetting failure of the upstream meniscus.[13,15,38] Upstream instabilities are associated with holes or air bubbles in the coating layer, temporal variations of the layer thickness "dripping" (drops spraying from the die), and in some cases also rivulets.[13,53] Instabilities induced by dewetting and deposition processes have not been studied for slot-die coating but for related coating processes, e.g., for dip coating,[16,22,39,40] where pattern formation also has been reported.

Lin et al.[33] employ numerical simulations to predict the parameters for homogeneous coating and find different types of coating defects outside the coating window. At high coating speeds, structures referred to as "breaklines" (lines of varying shape and width) coupled with dripping are observed, while rivulets, ribbing, and air entrainment limit the coating window if the flow rate is too low for the chosen coating velocity. Only stripes parallel to the coating direction are observed by Lin et al.[33] In terms of coating speeds, the predicted coating window is larger than the experimentally determined one. Kang et al.[41] find that the coating velocity has a dominant effect on both the thickness and the width of the stripes. The thickness is proportional to the velocity, while the width is inversely proportional to it. Khandavalli and Rothstein[35] study the impact of shear-thickening of the coating fluid on the stability of slot-die coating. The slot velocity for the onset of coating defect occurrence and the type of coating defect are examined at different coating parameters, such as the flow rate and coating gap height. They find that shear-thickening has a negative impact on the coating window and the intensity of the rivulet instability is found to increase with the shear-thickening magnitude.

Certain specific characteristics of the described patterning processes in slot-die coating are shared by the other above-mentioned

coating and deposition techniques, i.e., dip coating, Langmuir–Blodgett transfer, and evaporative dewetting.[16,17,24,29,30] These processes are normally employed to coat small areas. A recent detailed analysis of patterns obtained in evaporative dewetting is given by Jabal et al.[42] In the case of the well-studied "passive systems," the contact line velocity is selected by the system and not externally imposed as in "active systems" like slot-die coating and many other coating processes.[16] The latter are studied for simple and some complex liquids, e.g., for spin coating[43] and dip coating (also called "dragged plate geometry");[22,44] however, they are normally not suitable for large-scale industrial application. Besides the good availability of experimental results for these systems, the modeling of pattern formation is quite advanced. Thin-film models, i.e., hydrodynamic long-wave models and amended Cahn–Hilliard models, are used to analyze the bifurcation behavior of pattern formation processes in evaporative dewetting,[25] dip coating,[19,40,45] and Langmuir–Blodgett transfer.[23,46] Normally, this is done for one-dimensional substrates, but first results also exist in the two-dimensional case (see Refs. 47 and 48 and Sec. 8.2 of Ref. 49). Comparison of results for slot-die coating with other coating and deposition techniques will allow one to identify universal features of the occurring instabilities and patterning processes.

Here, we focus on an experimental study of pattern formation outside the coating window for slot-die coating. We demonstrate the existence of stripes oriented parallel and perpendicular with respect to the coating direction. Mixed patterns do also occur. The conditions of onset of pattern formation are discussed as well as the dependencies of the properties of the patterns on the experimental control parameters. The experimental findings are compared to theoretical results obtained using a long-wave hydrodynamic model for the slot-die coating of a partially wetting liquid. It takes capillarity and wettability into account as well as parameters of the coating process, such as coating velocity and gap height.

Our work is structured as follows. In Sec. II, the experimental setup is introduced, while Sec. III presents the corresponding results. Therein, the first subsection focuses on general coating scenarios, while another subsection discusses the influence of the coating gap height. Section IV introduces the employed model and describes the obtained results. Finally, we present a general discussion and conclusion in Sec. V. In addition, in Appendix B, we briefly discuss patterns induced by solvent evaporation.

II. EXPERIMENTAL SETUP
A. Coating system

To investigate the pattern formation occurring in slot-die coating, we employ as experimental model system the coating of a polyethylenterephthalat (PET)-substrate (Pütz GmbH, Germany) with a polyvinylpyrrolidon (PVP) K90 solution (VWR International GmbH, Germany; CAS: 9003-39-8, molecular weight: 360 000 g/mol, and K value range: 90–103) in ethanol. PET-substrates are very promising for low-cost applications in flexible electronics and in solar cells. The PVP–ethanol mixtures allow for a rather flexible adjustment of the physical characteristics of the coated liquid by varying the PVP content. Figure 1 presents the experimental setup and a schematic representation of a cross section of the essential part of the slot-die, the liquid inflow, and coated layer. The coater (Easycoater, Coatema Machinery GmbH, Germany) is a discontinuous coater for single piece coating. Compared to roll coating used in most other studies, the
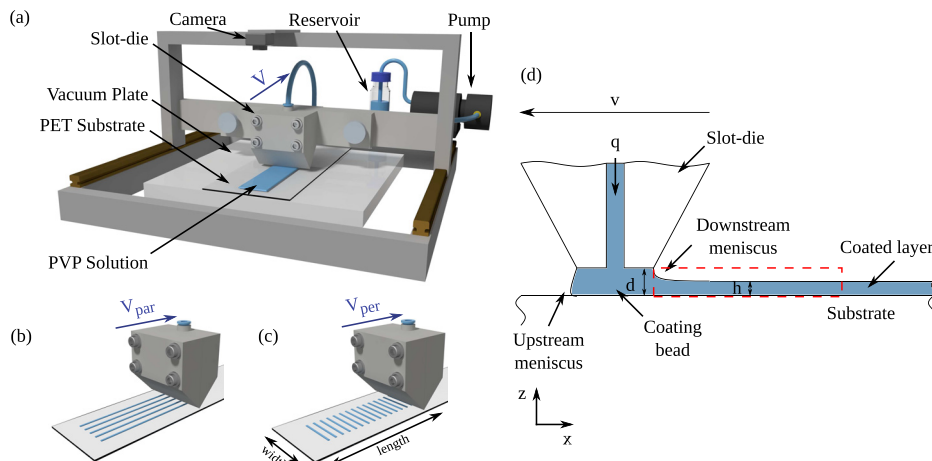
FIG. 1. (a) Experimental setup of the slot-die coater with a video camera for capturing the coated thin-film and the formation of stripes with (b) parallel and (c) perpendicular orientation with respect to the coating direction. (d) Schematic representation showing a cross section of the essential part of the slot-die, the liquid inflow, and coated layer.

discontinuous coater has the advantage that no part of the substrate is re-used as happens when the same part of the roll returns after each full turn. In contrast, in each slot-die experiment, reproducibly a fresh unused substrate is coated. Furthermore, it offers a fast and simple method to study slot-die coating on a small scale with a low waste of substrates and chemicals.

The coating die can move across the substrate at a constant velocity v in the x-direction, while liquid is pumped at a constant flow rate q through a thin channel (or slot) within the die. The slot-die is positioned at a controlled distance $d = 220\,\mu m$ (in z-direction) above the substrate, which we refer to as the *coating gap height*. The thin outlet of the channel at the tip of the slot-die has a fixed rectangular cross section of side lengths $100\,\mu m \times 8\,cm$ (in the $x \times y$ plane).

B. Coating layers

We distinguish between the *width* and the *length* of the coating area, as illustrated in Fig. 1(c). The width of the coating area (transversal size, y-direction) corresponds to the length of the slot in the coating die, i.e., it has a maximum width of 8 cm. The maximum length of the coating area (longitudinal size, x-direction) is about 25 cm.

Careful measurements of the coating gap height d have revealed that the gap has a small variance of approximately $\pm 30\,\mu m$ across the full length of the coating layer. For instance, at the start point ($x = 0\,cm$), the coating gap height is $d = 191\,\mu m$, while at the end point ($x = 25\,cm$), it is $d = 254\,\mu m$, which corresponds to an average slope of less than 2×10^{-4} rad. We consider this small imperfection of the experimental setup inevitable, as it results mostly from the adjustment of the vacuum plate, which holds the substrate, and the thermal expansion of the linear guide of the slot-die. To reduce the effect of the variance in the gap height, we only use the central third of the coating length for our analysis, i.e., length of approximately 8 cm. This also excludes possible transient effects of the unavoidable acceleration and deceleration phases of the coating die at the very start and end of the process. The remaining variation of the gap height in the central third of the coating area is in all experiments less than 10% of the coating gap height.

Since a variation of the coating gap height has been reported to have an influence on the pattern formation in some coating systems,

e.g., for confined dip coating,[50] the effects of variations in the coating gap height d on the pattern formation in our experimental setup are evaluated later in this work and seem to have only a small impact. As discussed in Sec. III B, one needs a relatively large change in the gap height to qualitatively alter the observed patterns. For instance, a parallel stripe pattern appears to be robust as it even remains qualitatively unchanged when the gap height is changed by a factor of three (from $d \approx 400\,\mu m$ to $d \approx 1200\,\mu m$). However, the gap height variation is observed to influence the pattern wavelength. As the variation in d along the length of the coating area is significantly smaller, we conclude that this deficiency in the experimental setup is acceptable.

In contrast to the variation of the gap height d along the *length* of the substrate, there is no measurable variation along the *width* of the coating area, i.e., the die is very well aligned parallel to the substrate.

The pattern formation is analyzed during the coating process by means of the CCD camera (VRmC PRO, VRmagic GmbH, Germany) installed directly on the die. Later, after finishing the coating process, the resulting pattern is analyzed via high-resolution photographs (OM-D E-M10 Mark III with macro objective, Olympus, Japan). Comparing the results of the two methods, we find that the already deposited pattern does not noticeably change (e.g., due to ethanol evaporation) during the remaining time of the coating process or shortly thereafter. However, on a much larger timescale, solvent evaporation results in a slight modulation of the thickness of the coated stripes, see Appendix B. In contrast, the width and arrangement of the coated stripes (i.e., the coated pattern described in Sec. III) remain unchanged. Further, a small concentration of blue ink is added to the ethanol–PVP mixtures to increase the optical contrast needed for imaging. No differences in the patterns and their characteristics, such as contact angle and viscosity, are observed in runs with and without ink. Therefore, the influence of the ink on the properties of the mixture can be neglected.

C. Coating fluid characterization

As coating liquid, we employ 5%–9% PVP solutions. We consider them to be nearly Newtonian: Although Goodwin and Hughes[51] use a 12% PVP solution as an example of a shear-thinning liquid and give in their Fig. 1.5 the behavior for a shear rate ranging from 0 to

$600 \, \text{s}^{-1}$, the power-law behavior is rather weak. While their fit indicates a power of 0.86, a linear (i.e., Newtonian) fit shows only a small deviation from their curve (see Appendix A).

It is important to note that not only the viscosity (as expected and originally intended) but also the contact angle of the ethanol–PVP mixture on the PET substrate is found to depend quite strongly on the polymer concentration. We use a setup built in-house and an ImageJ plugin[52] to fit the shape of static sessile droplets after inflation with a syringe and measure the advancing contact angle from the video data. The resulting dependencies of the contact angle and the viscosity on PVP concentration are presented in Fig. 2. The measured viscosity in cP corresponds to $1 \, \text{cP} = 10^{-3} \, \text{Pa s}$. Changing the mass concentration of PVP from 2% to 12%, the viscosity increases 50-fold, while the contact angle increases threefold from about 17° to about 50°. Although, considering Young's law, a change in the equilibrium contact angle could result from dependencies of the liquid–gas and the liquid–solid interface tensions on the PVP concentration, the liquid–gas interface tension of PVP-in-ethanol solutions is known to only slightly depend on the concentration. Reference 53 reports a decrease from $\sigma \approx 24$ to $23 \, \text{mN/m}$ for an increase in the PVP concentration from 0% to 20%. In consequence, the observed adaption of the contact angle to the concentration must be due to a strong dependence of the liquid–solid interface tension on the concentration.

D. Parameter space

The pattern topology and quantitative characteristics, such as typical pattern length scales, are potentially influenced by several processing parameters, e.g., the coating velocity v, the coating gap height d, the viscosity of the liquid mixture η, its surface tension σ, and the liquid flow rate q. As the principal parameter of our study, we systematically vary the coating velocity v and measure the critical velocities at which transitions between the patterns are observed. While the coating velocity is kept constant for each individual run, the velocity is varied between the experiments from $v_{\text{min}} = 0.4 \, \text{m/min}$ to $v_{\text{max}} = 4.4 \, \text{m/min}$ in steps of $0.2 \, \text{m/min}$.
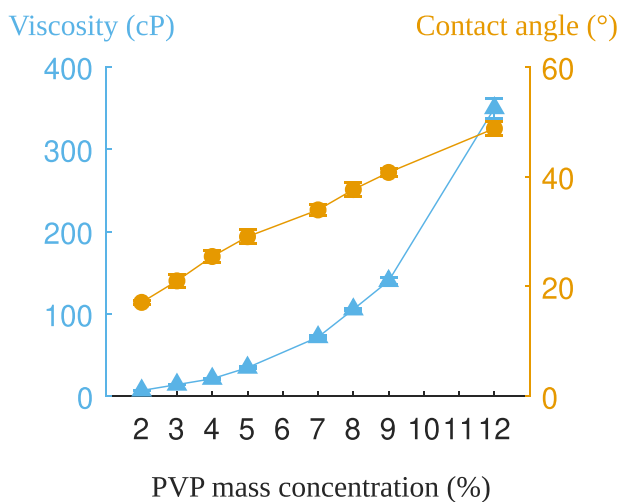

FIG. 2. Viscosity of the ethanol–PVP mixture (left vertical axis, triangles) and advancing contact angle in degree (right vertical axis, circles) as functions of the mass concentration of PVP in the solution.

As a second parameter, we control the mass concentration of PVP in the coating fluid and, consequentially, the viscosity η of the liquid. Note, however, that as a side effect, this also influences the equilibrium contact angle θ, while the liquid surface tension σ is close to constant, as discussed in Sec. II C. The experimentally considered viscosities range from $\eta = 7 \, \text{cP}$ to $\eta = 350 \, \text{cP}$. Together with the coating velocity, this spans a two-dimensional parameter space (v, η), which we later map onto the space spanned by the dimensionless Capillary and Reynolds numbers (Ca, Re).

The gap height is usually fixed at $d = 220 \, \mu\text{m}$ throughout this work, except for the case study at the end of Sec. III (Figs. 8 and 9), where we evaluate the effects of variations in the gap height on our results. There, experiments are performed for various gap heights in the range from $d = 220 \, \mu\text{m}$ to $d = 1210 \, \mu\text{m}$. The liquid flow rate $q = 4.8 \pm 0.2 \, \text{ml/min}$ (or $1 \, \text{mm}^2/\text{s}$ per unit width) in the slot-die is kept constant at all times.

III. EXPERIMENTAL RESULTS
A. Coating scenarios

Depending on the parameters, homogeneous as well as inhomogeneous coatings are deposited on the substrate. In general, four types of coating patterns are observed in addition to the uniform coating. They are as follows:

1. parallel stripes oriented perpendicular to the direction of coating [Fig. 3(a)];
2. parallel stripes oriented parallel to the direction of coating [Fig. 3(b)];
3. irregular mixed patterns, corresponding to a combination of parallel and perpendicular stripes [Fig. 3(c)];
4. irregular patterns, corresponding to a set of rather randomly located dots with tail-like structures in the direction of the die motion [Fig. 3(d)].

The mixed patterns consist of areas covered by stripes of different orientation, i.e., the stripes in different substrate regions are perpendicular to each other. This mixed-pattern regime is observed in a parameter range at the border between the parameter regions, where parallel and perpendicular stripes occur, respectively. Note that sometimes the perpendicular stripes are slightly tilted with respect to the direction of coating. Because the tilt angle differs between the runs [cf., e.g., Figs. 3(a) and 3(c)], we believe the effect is not due to imperfections in the gap height, but rather represents spontaneously occurring defects (phase slips) in the line pattern.

Figure 4(a) shows a morphological phase diagram indicating where the various coating types and patterns occur in the parameter plane spanned by coating velocity v and viscosity η. In general, at low velocities and low viscosities, the coating is homogeneous, i.e., the substrate is covered by a liquid layer of constant thickness. This parameter region is also known as the coating window. With increasing velocity, a transition occurs from the homogeneous coating to coating defects due to an instability of the meniscus. Thus, the red curve marked by blue open squares corresponds to the critical coating velocity $v_{\text{crit,hom}}$ in dependence of viscosity. At high velocities and high viscosities above $v_{\text{crit,irregular}}$, irregular patterns prevail. The particular transition scenario found when going from one to the other limiting case depends on the liquid viscosity. The images in the three rows of
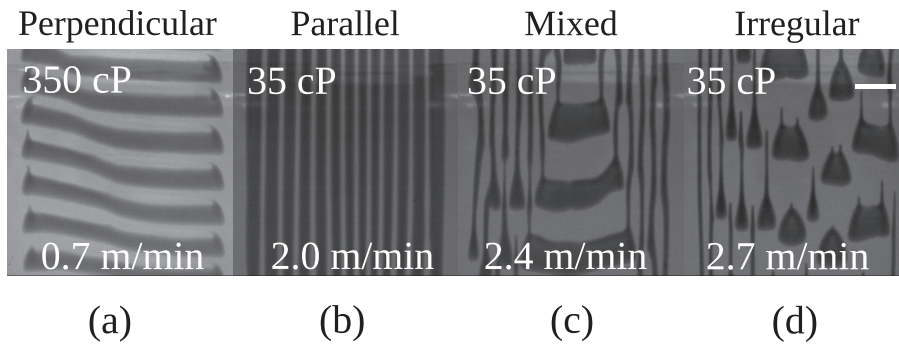
Perpendicular	Parallel	Mixed	Irregular
350 cP	35 cP	35 cP	35 cP
0.7 m/min	2.0 m/min	2.4 m/min	2.7 m/min
(a)	(b)	(c)	(d)

FIG. 3. Images of (a) stripes oriented perpendicular to the direction of coating, (b) stripes oriented parallel to the direction of coating, (c) a mixture of stripes perpendicular and parallel to the direction of coating, and (d) an irregular pattern. The viscosity and coating velocity are given in the images. Dark areas represent the coating, while lighter areas correspond to the bare substrate. The scale bar is 10 mm (top right). The arrow on the right indicates the coating direction.

Fig. 4(b) show typical transitions in the observed patterns at fixed high, intermediate, and low viscosity, respectively.

Inspecting the first row in Fig. 4(b), one observes that at high viscosities (or high contact angles, cf. Fig. 2), with increasing v the homogeneous coating (e.g., at $v_{crit,hom} = 0.5$ m/min) is replaced by perpendicular stripes (e.g., at $v = 0.7$ m/min) that can be slightly bent at the lateral sides of the coating area. The stripes are horizontal in the figure as the slot-die is horizontal with respect to the panels and moves vertically upward across them (as indicated by the arrow). Upon further increase in v, the stripes break up by the subsequent introduction of phase slips (e.g., at $v = 1.2$ m/min). Ultimately, the pattern becomes quite irregular and consists partly of dots that can be slightly widened in the direction perpendicular to the coating direction (e.g., at $v_{crit,irregular} = 1.5$ m/min). In contrast, at low viscosity [bottom row in Fig. 4(b)], with increasing v the homogeneous coating (e.g., at $v_{crit,hom} = 2.5$ m/min) is replaced by parallel stripes (e.g., at $v = 3.1$ m/min). Upon further increase in v, the stripes first develop

asymmetric bulges that at larger v develop into defects where stripes split or end (e.g., at $v = 3.9$ m/min). Toward larger velocities, stripes mostly end at bulges. Ultimately, only the bulges survive, showing short stripe-like appendices and the pattern becomes quite irregular (e.g., at $v_{crit,irregular} = 4.3$ m/min). Overall, the transition to patterns occurs at larger velocities in the low viscosity case than in the high viscosity case [cf. Fig. 4(a)].

In a small velocities range at the intermediate viscosity, one observes the simultaneous occurrence of perpendicular and parallel stripes in different regions of the substrate [see the second row in Fig. 4(b)]. The transition scenario for the intermediate viscosity, e.g., $\eta = 35$ cP and $\eta = 72$ cP at 5% and 7% of PVP, respectively, is shown in Fig. 5. At $\eta = 35$ cP, the homogeneous coating first destabilizes to parallel stripes. With increasing velocity, patches of perpendicular stripes appear within the pattern of parallel stripes. At $\eta = 72$ cP, as the coating velocity is increased, the homogeneous coating is destabilized and first pieces of perpendicular empty stripes appear
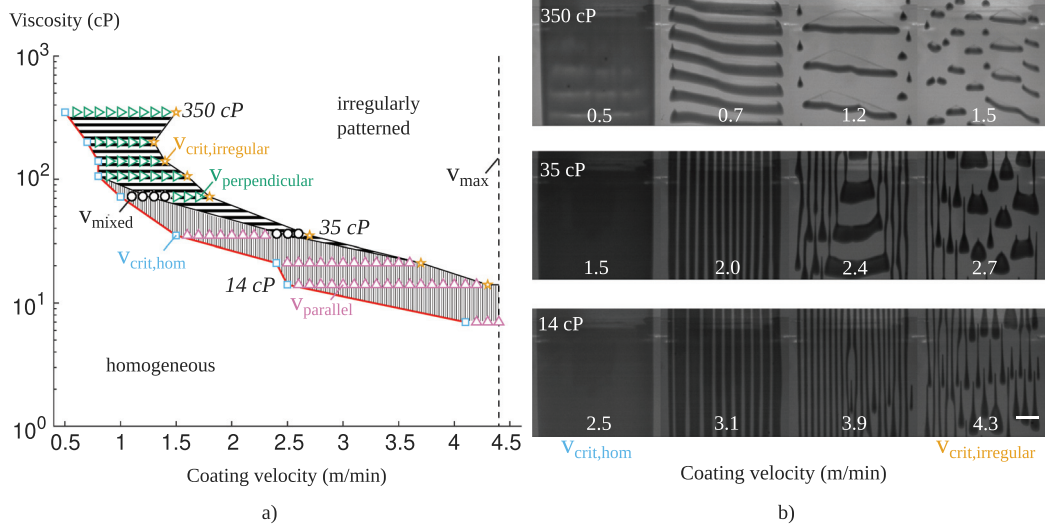

a)

b)

FIG. 4. (a) The morphological phase diagram presents the parameter regions corresponding to the various coating patterns in the plane spanned by coating velocity v and viscosity η. The region corresponding to homogeneous coating is at velocities $v \leq v_{crit,hom}$ (limited by squares and the red line), irregular patterns occur at velocities $v \geq v_{crit,irregular}$ (limited by stars). Parallel (marked as Δ) and perpendicular (marked as $\triangleright$) stripes are found at $v_{parallel}$ and $v_{perpendicular}$, respectively, and mixed patterns at v_{mixed}. Vertically and horizontally hatched regions mark the occurrence of parallel and perpendicular stripe patterns, respectively. (b) Transitions from homogeneous coating to stripes upon increasing the coating velocity for three different viscosities. The coating direction in the figures is from the bottom to the top as indicated by the arrow at the right, and the scale bar is 10 mm.
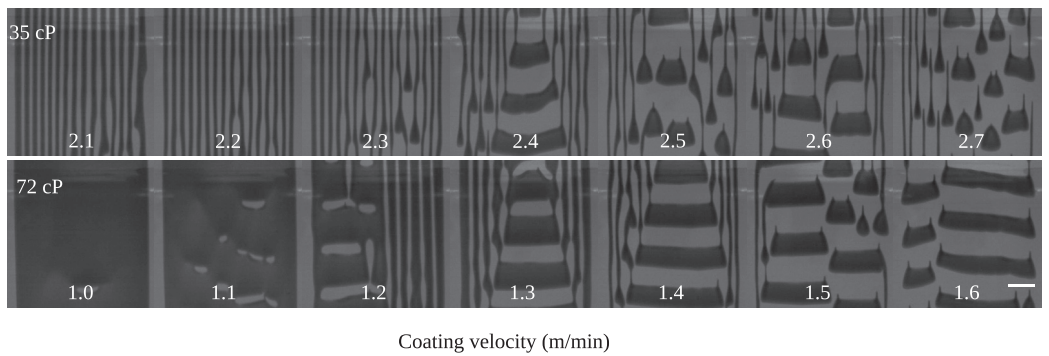
FIG. 5. Typical transition scenario of coating patterns in dependence of the coating velocity v at fixed intermediate viscosities $\eta = 35\,\mathrm{cP}$ and $\eta = 72\,\mathrm{cP}$. With increasing v, a transition occurs to coexisting perpendicular and parallel stripes and further to perpendicular stripe patterns with defects. Remaining details are as in Fig. 4.
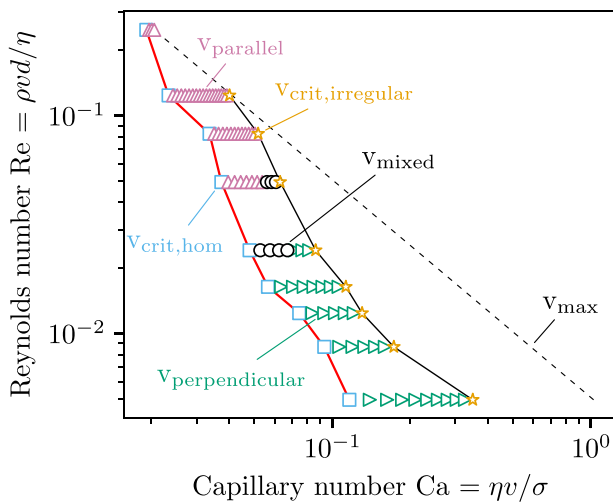

FIG. 6. The data of the phase diagram in Fig. 4(a) shown in the plane spanned by the Capillary and Reynolds numbers. All colors and markers are as in Fig. 4(a).

($v = 1.1\,\mathrm{m/min}$). Further increasing v, the stripe-shaped holes grow in length until resembling a perpendicular stripe pattern. However, in part of the coating area, regions of parallel stripes also develop ($v = 1.2, \ldots, 1.4\,\mathrm{m/min}$). At intermediate velocities, areas filled with parallel and perpendicular stripes seem to coexist in every individual coating experiment. At higher velocities, perpendicular stripes dominate before breaking up via phase slips as described above.

Further, we have converted the data of the phase diagram in Fig. 4(a) to dimensionless quantities, to allow for a more general comparison with other related experiments of coating instabilities. As typically found in the literature,[11,54,55] we choose the Capillary number $\mathrm{Ca} = \eta v/\sigma$ and the Reynolds number $\mathrm{Re} = \rho v d/\eta$ to span the phase plane for the rescaled diagram in Fig. 6. Here, we find that the observed instabilities occur in a laminar regime ($\mathrm{Re} \ll 1$), and both the Reynolds number and the Capillary number are involved in the selection of the pattern.

For all performed experiments with a clear stripe pattern, the period of the stripes in the central (nontransient) coating area of approximately 8 cm length is measured. The dependence of the wavenumber $k = 2\pi N/L$ of the stripes on the coating velocity is presented in Figs. 7(a) and 7(b) for the perpendicular and parallel stripes,
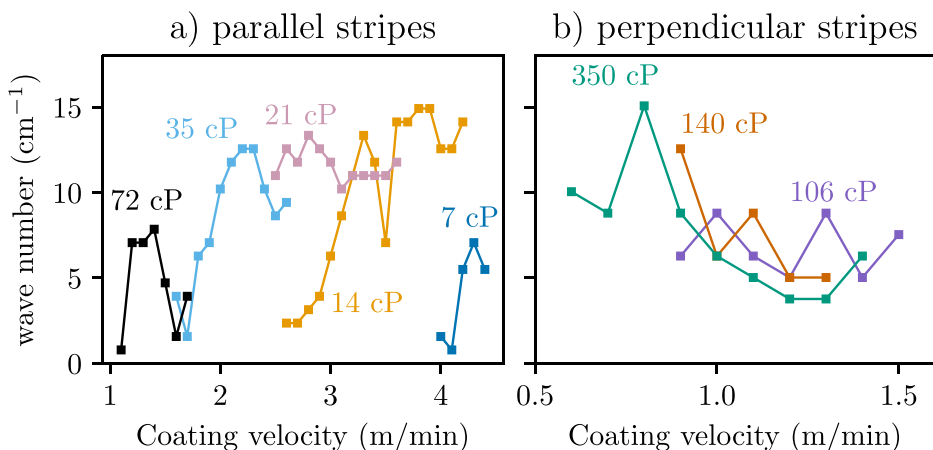

FIG. 7. (a) The wavenumber of parallel stripes and (b) the wavenumber of perpendicular stripes in the central coating area are given in dependence of the coating velocity at different viscosities.

respectively, where L denotes the extent of the stripe covered region. The perpendicular stripes observed at high viscosity (cf. Fig. 4) show (up to an outlier) a decreasing wavenumber (proportional to the inverse period of stripe patterns). The behavior is different for the parallel stripes, where the wavenumber increases with the velocity.

B. Influence on the coating gap height

Next, we study the influence of the coating gap height by stepwise increasing it at a fixed coating velocity $v_{crit,hom}$, which is the largest velocity for which a homogeneous coating is achieved for a given viscosity at the lowest considered gap height. This ensures that we are always within the parameter range where patterns occur. In this way, we can also assess which influence small changes in the gap height have (like the variation related to the above-discussed small imperfectness in the experimental setup). This procedure is followed for a number of different viscosities.

Figure 8(a) gives an overview of the conducted experiments and the resulting patterns. When the coating gap height is increased above a critical value $d_{crit,hom}$, a transverse destabilization of the meniscus is observed and the homogeneous coating breaks up into stripes parallel to the coating direction. Unlike the observations made above when increasing the coating velocity, here the orientation of the stripes remains unchanged when increasing the viscosity. Also, there is no pronounced influence of viscosity on the onset of pattern formation, i.e., on $d_{crit,hom}$, see Fig. 8(a).

With increasing coating gap height, the distance between stripes increases and their width decreases. This occurs at all tested viscosities, see the example patterns in Fig. 8(b).

At 9% PVP, which corresponds to $\eta = 140$ cP, a few perpendicular stripe-shaped holes appear in the otherwise homogeneous coating when increasing the coating gap height, see the white arrow in the leftmost image of Fig. 9. Here, we vary the gap height d for one fixed combination of the parameters v and η, where only stripes perpendicular to the coating direction appear when increasing the coating gap height. However, these stripes are irregular and not as well defined as the stripes parallel to the coating direction, which appear when increasing the coating gap height at the other viscosities.

Again, the results may be converted to a dimensionless form when the gap height d is rescaled by a characteristic reference length scale. We follow Carvalho and Kheshgi[11] and compare the gap height to the film height of a homogeneous coating $h_{hom} = q/(sv)$ for a given flow rate q and slot width s. This results in a dimensionless gap height $\tilde{d} = dsv/q$, which ranges from 1.4–16.1 in the experiments depicted in Fig. 8.

IV. THEORETICAL APPROACH

To compare the presented experimental results to theory, we introduce a long-wave hydrodynamic model[56–58] for slot-die coating of a simple partially wetting nonvolatile liquid on a rigid solid homogeneous substrate. It takes capillarity and wettability into account as well as parameters of the coating process, such as the coating velocity and gap height. We focus on the region close to the downstream meniscus, i.e., on the region directly trailing the moving coating die. Similar models are successfully employed to describe the meniscus dynamics and instabilities for related coating techniques, such as dip-coating.[39,40,59–61]

The evolution equation for the film thickness profile $h(\mathbf{x}, t)$ is obtained by a long-wave expansion of the Navier–Stokes equations in a laminar flow limit together with adequate boundary conditions at the solid substrate and a free surface.[56,57] Here, we adapt the resulting equation to the geometry of slot-die coating in the reference frame of the meniscus, i.e., moving with the coating die. In dimensional form, it reads
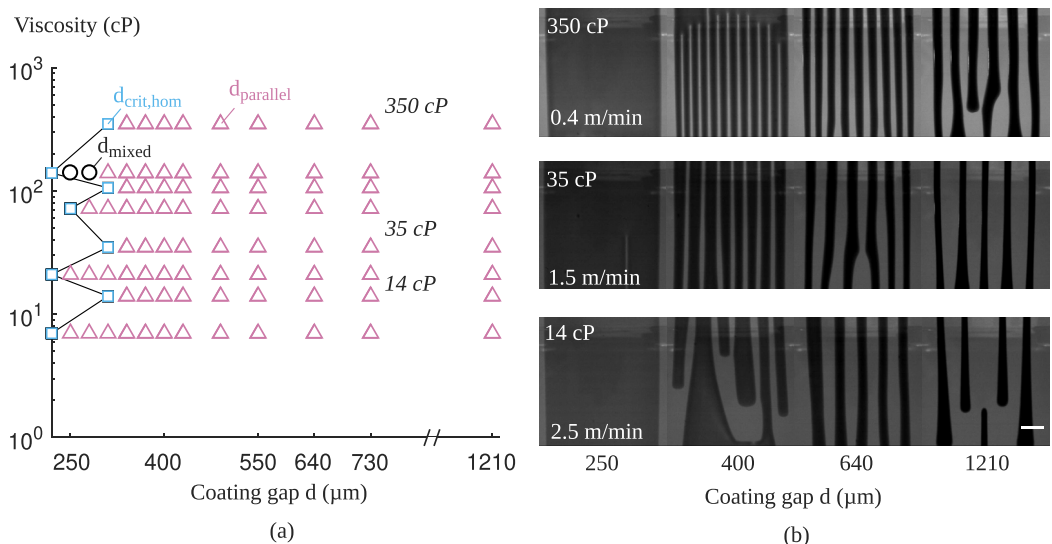
FIG. 8. (a) Morphological phase diagram for the parameters corresponding to the transition from homogeneous coating to stripes upon increasing the coating gap height d, starting from $d = 220$ μm. The velocity used for each viscosity is $v_{crit,hom}$ (see Fig. 4). (b) Transition of patterns with increasing d at different fixed viscosities. Remaining details are as in Fig. 4.

$$\frac{\partial}{\partial t} h(\mathbf{x}, t) = -\nabla \cdot \mathbf{j}(\mathbf{x}, t) = -\nabla \cdot \left[\frac{h^3}{3\eta} \nabla(\sigma \Delta h + \Pi(h)) \right] - v\, \partial_x h,$$

(1)

where $\mathbf{j}$ is the liquid flux, and the advection term with coating velocity v accounts for the movement of the slot-die over the substrate. Moreover, $\Pi(h)$ is the Derjaguin or disjoining pressure that models partial wettability.[62–64] We employ the common form

$$\Pi(h) = H_A \left(\frac{h_p^3}{h^6} - \frac{1}{h^3} \right)$$

(2)

that combines a destabilizing long-range van der Waals interaction and a short-range stabilizing interaction. Here, it is parametrized by the height of the equilibrium adsorption layer h_p and the Hamaker constant $H_A = \frac{5}{3} \sigma h_p^2 \theta^2$ that we relate to the equilibrium contact angle θ employing Young's law.[65] Since Eq. (1) describes the evolution of the height profile of the coated film, we limit the spatial domain to the red box in Fig. 1. That is, on the downstream side, the position $x = 0$ marks the edge of the slot-die and gives the limiting point of the downstream meniscus. The experimental gap height d and imposed constant liquid influx q then translate into the boundary conditions,

$$h(x = 0, t) = d \quad \text{and} \quad \mathbf{j}(x = 0, t) = \frac{q}{s} \hat{\mathbf{e}}_x,$$

(3)

where s is the length of the slot. We place the opposite boundary of the domain at a position $x = L$ far from the meniscus and apply the Neumann condition

$$\frac{\partial}{\partial x} h(x = L, t) = \frac{\partial^3}{\partial x^3} h(x = L, t) = 0$$

(4)

that allows for free outflow of the liquid volume.

We rewrite the model in dimensionless quantities (with tilde). This prepares the equations for a numerical treatment and provides insight into the scaling behavior of the dynamic states with respect to the parameters. In particular, we choose the gap height as the reference height scale $h_0 = d$ and introduce the length scale $x_0 = \sqrt{3/5}\, d/\theta$ and timescale $t_0 = 27\eta d/(25\sigma\theta^4)$ such that the dimensionless governing equation reads

$$\frac{\partial}{\partial \tilde{t}} \tilde{h}(\tilde{\mathbf{x}}, \tilde{t}) = -\tilde{\nabla} \cdot \left\{ \tilde{h}^3 \tilde{\nabla} \left[\tilde{\Delta} \tilde{h} + \tilde{h}_p^2 \left(\frac{\tilde{h}_p^3}{\tilde{h}^6} - \frac{1}{\tilde{h}^3} \right) \right] \right\} - \widetilde{Ca}\, \partial_{\tilde{x}} \tilde{h}.$$

(5)

Here, the number of free parameters is reduced to a scaled Capillary number $\widetilde{Ca} = 27\sqrt{5}\, \eta v / (25\sqrt{3}\, \sigma\theta^3)$, the dimensionless flow rate $\tilde{q} = q\, t_0/(x_0 h_0)$, and the (typically small) ratio of the adsorption layer thickness to gap height $\tilde{h}_p = h_p/d$, which we fix at $\tilde{h}_p = 0.04$.

We employ direct numerical simulations of the model equations (1)–(4) using the finite element method (FEM) approach of the C++-library OOMPH-LIB[66] and a backward differentiation scheme of second order (BDF2) for time integration. The simulations are performed on a spatial domain of the size $5 \times 2.5\, \text{mm}^2$ with periodic boundaries in the y-direction. The periodic boundary conditions can cause defects in the coating patterns when the lateral domain size does not match the natural wavelength of a parallel stripe pattern. Modeling our experimental setup, we fix the gap height at $d = 220\, \mu\text{m}$, impose a flow rate $q = 4.8\, \text{ml/min}$ for a slot of length $s = 8\, \text{cm}$, and assume a surface tension of $\sigma = 25\, \text{mN/m}$. Additionally, the contact angle is adapted to the viscosity by interpolating the data of the measurement presented in Fig. 2 (i.e., $\theta = 17°$ for $\eta = 3\, \text{cP}$, $\theta = 23°$ for $\eta = 7\, \text{cP}$ and $\theta = 38°$ for $\eta = 42\, \text{cP}$, i.e., the contact angle increases with the viscosity). The simulation is initialized with a static tanh-shaped meniscus that interpolates between the boundary condition $h(x = 0) = d$ and the "dry" adsorption layer $h(x = L) = h_p$ plus a weak transverse modulation of long wavelength. After numerically integrating the governing equations until transient effects have disappeared, we observe homogeneous coating layers as well as the formation of various stripe and droplet patterns at the meniscus. In analogy to Fig. 4, we show in Fig. 10 the transition between these patterns for representative configurations of the coating speed and the viscosity.

In agreement with the experiment, at low velocities of the coating die, we obtain homogeneously coated films (e.g., see $v = 1.5\, \text{m/min}$ in Fig. 10). The height of the coated layer far from the meniscus is $h_{\text{hom}} = q/(sv)$, as expected due to the conservation of liquid volume. As in the experiments, in the calculations this homogeneous coating becomes unstable when the velocity increases above a critical value, i.e., when the coating height h_{hom} decreases below a critical value. Similarly, the same instability is observed at lower coating speeds when the viscosity becomes large, since both the viscosity and the coating speed enter the Capillary number in the dimensionless dynamics [Eq. (5)]. Beyond the instability threshold, a stripe pattern emerges, which is oriented perpendicular to the coating direction. In the column with $v = 2.9\, \text{m/min}$ in Fig. 10, we observe that the wavelength of the pattern decreases with increasing viscosity. This is due to the change in the contact angle with the viscosity and therefore due to a change in the length scale x_0 in the dimensionless dynamics.

When the coating speed is further increased to $v = 3.6\, \text{m/min}$, the meniscus shows an additional transversal instability that leads to the periodic formation of droplets instead of stripes, resembling, e.g., the transition shown in the top row of Fig. 4(b), where droplets are found when the velocity exceeds $v_{\text{crit,irregular}}$. In the simulations, we see no significant dependence on viscosity in the critical coating speed
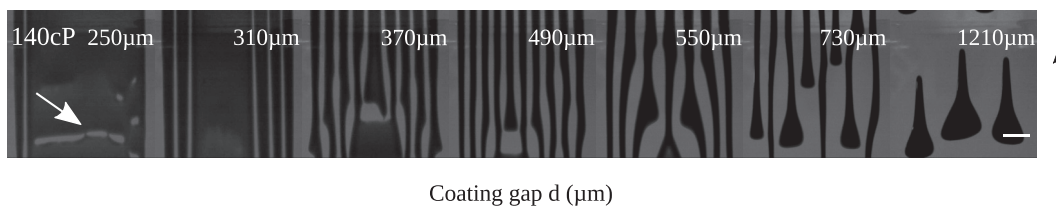
Coating gap d (µm)

FIG. 9. Transition from homogeneous coating to stripes upon increasing the coating gap from $d = 250\, \mu\text{m}$ to $d = 1210\, \mu\text{m}$ as given in each image with $v = 0.7\, \text{m/min}$ for $\eta = 140\, \text{cP}$. Remaining details are as in Fig. 4.
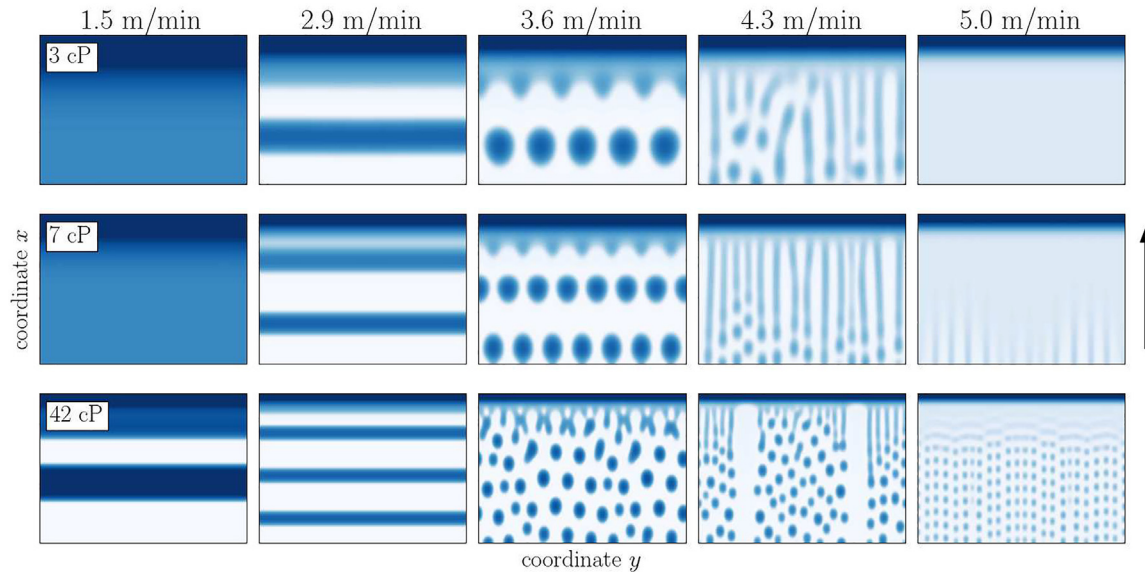
FIG. 10. Snapshots of numerical simulations of the model equation (1) for various combinations of the viscosity and the coating speed after initial transients. Blue colors represent the liquid, while uncoated areas are white. The slot is positioned at the top of the domain (5 × 2.5 mm²) and moves upwards. Similar to the experimental results (cf. Fig. 4), we find transitions between a homogeneous coating and different stripe and droplet patterns that strongly depend on the coating speed and viscosity. The arrow indicates the coating direction. Further details are discussed in the main text.

of this transition. As for the stripe pattern, viscosity influences the wavelengths of the drop patterns. In the vicinity of the transition, the system may show long transients or intermittent/mixed behavior, where bursts of drops and stripes can be observed concurrently. In this regime, finite size effects and perturbations may play an important role in the selection of the pattern.

At even larger coating speeds, fingers of liquid can grow from the meniscus and thus form a stripe pattern that is oriented parallel to the coating direction (e.g., see $v = 4.3$ m/min). These stripes will break up into single droplets if they become too long, and also defects may be induced if the lateral width of the (periodic) domain is incompatible with the wavelength. Regular stable regimes exist for selected domain sizes. Again, the wavelength is observed to scale with the viscosity. An increase in the viscosity also increases the equilibrium contact angle parameter in the model (as both are linked to the PVP concentration in the experimentally used liquid). In our dimensional analysis, the length scale x_0 is found to scale inversely with the contact angle. Consequentially, a decrease in the (dimensional) pattern wavelength with increasing viscosity is reasonable in the model. If the wavelength of the parallel stripes is very small (e.g., for $\eta = 42$ cP), the pattern is interrupted by broad uncoated areas, while the meniscus confines the liquid into smaller regions, preserving the pattern. Again, transient/intermittent regimes between parallel stripes and droplet patterns can be found near the critical parameter values.

For relatively large velocities (e.g., $v = 5.0$ m/min), the effective coating layer height $q/(sv)$ is no longer large as compared to the adsorption layer height h_p. In this regime, the model reveals ultra-thin homogeneous coatings that are stable on small domains, but show dewetting behavior if the domain is large enough compared to the wavelength of the dewetting instability (see Ref. 57). Accordingly, we see a stable layer for $\eta = 3$ cP, a lateral dewetting instability for

$\eta = 7$ cP, and dewetting toward droplets for $\eta = 42$ cP. We stress that these patterns do not result from an instability at the meniscus and depend on the choice of the wetting potential.

We also note that in the simulation, we always first find a transition from a homogeneous film to perpendicular stripes, while in the experiment, this only occurs at large viscosities. Furthermore, there is a slight quantitative mismatch in the scales of the simulation and the experiments. Therefore, in Fig. 10, we have chosen the parameters such that a good overview is given of the patterns that can be observed in the long-wave hydrodynamic thin-film model. The discussion of these deviations is continued in Sec. V.

Finally, we mention that the occurrence of perpendicular stripes at small velocities is a rather robust result. It is found for various initial conditions, in particular, transversal modulations of varying strengths and wavelengths, but none of these could stabilize other patterns than perpendicular stripes near the onset of pattern formation at low velocities. When a state of parallel stripes obtained at higher velocity is taken as initial condition, and the velocity is decreased, the state transitions toward perpendicular stripes via defects and/or mixed states.

V. DISCUSSION

We have analyzed the occurrence of patterned coatings in slot-die coating of thin layers of PVP–ethanol mixtures on a timescale where the influence of evaporation is neglectable. The mass concentration of PVP has been employed to vary the viscosity of the mixture, which also changes the contact angle of the liquid. The coating velocity and coating gap height have been used as further main control parameters. As a result, we have found that above a critical concentration-dependent coating velocity, the uniform coating becomes unstable with respect to patterning. At high concentrations (high viscosities), we have found stripe patterns oriented perpendicular to the coating

direction, while at low concentrations (low viscosities), stripes oriented in the parallel direction appear. In an intermediate case, the coexistence of both types of stripes is observed. Further increasing the velocity, in all three cases the patterns acquire more and more defects and finally become rather irregular. Additionally, pattern formation has also been observed when increasing the coating gap height. In this case, parallel stripes appear regardless of the concentration. We have found that the period of the stripe pattern decreases with increasing coating gap height.

These findings consistently expand results known from the literature. In particular, Raupp et al.[15] describe the formation of parallel stripes in a range of coating velocities as rivulets. A similar instability known as ribbing—a weak transversal modulation of film thickness[12]—has not been found here, possibly due to the low viscosity of the coating liquid or the specific geometry of the slot-die.[32] In particular, in Ref. 32, the occurrence of ribbing depends on the angle between the downstream lip of the slot-die and the substrate, which is low in their case. This could imply that the geometry of the slot-die, namely, the angle of the downstream lip, governs the ribbing instability. Schmitt et al.[36] find perpendicular stripes at high viscosities with parameter dependencies that qualitatively agree with our findings. Parallel and perpendicular stripe formation is also observed by Khandavalli and Rothstein[35] and Kang et al.[41] However, the coexistence of stripes in the two different directions has to our knowledge not yet been reported in the literature.

We have also presented results for the dependence of the period of stripe patterns on coating velocity. Overall, our experiments indicate that the wavenumber of the parallel stripe pattern depends strongly on the concentration and the coating velocity, where with increasing velocity the wavenumber first increases before it decreases again. While on the basis of the presented data, one cannot yet deduce the bifurcation character of the onset of pattern formation, a part of the behavior resembles the one observed in Langmuir–Blodgett transfer[22,46] and also in evaporative dewetting.[25] Qualitatively similar behavior is also observed in models of solute deposition by dip coating solutions with volatile solvent.[19,45] Note, however, that the comparison to the wider literature is limited by the fact that most of the model results in the mentioned works is for one-dimensional substrates only, i.e., most discussed patterns correspond to perpendicular stripes. The most complete results are found for Langmuir–Blodgett transfer. There, with increasing plate velocity, a transition from parallel to perpendicular stripes is found,[46] i.e., a case encountered here at intermediate viscosity. It is also found that the pattern wavenumber for the perpendicular stripes first increases and then decreases with transfer velocity[22]—a result consistent with our findings for parallel stripes. In our case of perpendicular stripes, the corresponding results are not fully conclusive as the small coating area does not provide a sufficiently good statistics. In evaporative dewetting, the contact line velocity is not externally controlled but results via the evaporation rate from the ambient humidity. In Ref. 25, only perpendicular stripes are considered. They show a wavenumber that predominantly decreases (increases) with increasing evaporation rate (solute concentration, i.e., viscosity).

In addition to the experimental results, we have also presented a basic long-wave hydrodynamic model describing the dynamics of the meniscus and deposited film. It describes the intricate interplay of capillarity and wettability with the motion of the die and the influx

strength. The resulting nonlinear dynamic model has allowed us to qualitatively reproduce main features of the experimentally observed patterns, thereby indicating that it is the nonlinear interplay of the included influences that results in patterning. We have obtained typical sequences of patterns as found when increasing the coating speed, namely, the transition from uniform coating to perpendicular stripes, droplets, and parallel stripes. However, the agreement is only partial, since there are both, qualitative and quantitative differences. Qualitatively, the thin-film model reproduces only part of the sequences of the various pattern types seen in the experiment. The modeling and the experiments agree in the transitions observed for high-viscosity mixtures, cf. Figs. 4 and 10, namely, the transition from homogeneous coating to perpendicular stripes, and at larger coater velocity the transition from perpendicular stripes to drop patterns. The decrease in the critical velocity $v_{\mathrm{crit,hom}}$ with increasing viscosity is also well captured. However, the experiments have also shown a direct transition from uniform layers to parallel stripes, while the model only shows direct transitions from a uniform layer to perpendicular stripes. Nevertheless, the model is able to reproduce all different experimentally observed patterns on comparable scales. A future in-depth bifurcation study could give further insight into all possible sequences of patterning including possible multistabilities of different pattern types. The presented model is minimal in the sense that the underlying physics cannot be further simplified without losing the pattern forming properties, i.e., the effects of driving, capillarity, and wettability cannot be neglected in the model.

In the dimensionless formulation of the model, one of the few remaining parameters is the Capillary number $\mathrm{Ca} = \eta v/\sigma$. While the Capillary number suggests that a change in viscosity η could have a similar effect as a change in coating velocity v, this does not reflect in our results. The model does not show a strong dependence of the dominant pattern on viscosity, mostly only the pattern wavelength changes. Similarly, in the experiment, the stability border of the homogeneous solution does not occur at a constant Ca (cf. Fig. 6). A fit to the stability border in Fig. 4 rather suggests that $v_{\mathrm{crit,hom}} \sim \eta^{-2}$. Hence, the Capillary number is not the only relevant dimensionless number in our phase diagram. We have accounted for the dependence on viscosity by additionally considering the Reynolds number $\mathrm{Re} = \rho v d/\eta$, although the Reynolds numbers in our experiment are generally low, i.e., the effect of inertia is rather weak. The employed thin-film model does not include inertial effects, which could be accounted for in future studies with more complex Navier–Stokes type models. The change in the pattern wavelength with viscosity occurs both in experiment and simulations and is potentially related to the dependence of the liquid contact angle on the PVP mass concentration, which is used to control the viscosity of the coating liquid in the experiment. The effect was also accounted for in our model via the employed wettability.

In the model, we have found that wettability, in particular, the height of the adsorption layer, is critical for achieving quantitative comparability of the observed length scales. Alongside the choice of the model parameters, the exact theoretical onset of pattern formation also depends on the functional form of the wetting potential, as it represents an important driving force of the contact line dynamics. Here, we have employed a common expression for the wetting potential. Using an alternate wetting potential (at fixed macroscopic contact angle and adsorption layer height) should, however, not lead to

qualitative differences in the patterns occurring in the simulations. We expect that the experimental and theoretical scales could be further aligned, if in the experiments wettability and viscosity could be independently adjusted, or alternatively, if the effects underlying the observed dependence were better understood and incorporated into the model. For a deeper analysis of the influences of viscosity and wettability in future investigations, it would be helpful to find experimental systems where the two parameters can be independently changed.

Further improvement could include a discussion of the influence of non-Newtonian effects in all stages of pattern formation, in particular, when local shear rates strongly deviate from the averaged values our above estimates rely on. This may include shear-thinning, stretching force, and viscoelasticity of the polymer solution as observed, e.g., for liquid jets.[67,68]

The research of Carvalho and Kheshgi[11] and Romero et al.[37] suggests that coating defects in the so-called low-flow limit may occur when the curvature of the downstream meniscus increases until it fails to bridge the coating gap height. Since our model only captures the height profile of the downstream meniscus, this effect is excluded from our theoretical description. To incorporate it into the model, one would need to include the hydrodynamics within the gap. Another discussed effect is the entrainment of air bubbles at the upstream meniscus in Fig. 1(d). The bubbles are then transported underneath the die to the downstream meniscus. However, this normally results in air bubbles enclosed in the coating, but not the coating patterns studied here.[14] Although the fluid dynamics at the upstream meniscus and under the slot are not accounted for, our model is still able to reproduce the rich variety of patterns observed experimentally. Hence, one key result of our theoretical approach is that also the dynamics of the coated film close to the downstream meniscus, including wettability, should be considered in future studies to fully understand the defects occurring in slot-die coating.

The importance of the flow under the die is confirmed by a further observation: To investigate the influence of solvent evaporation, a video camera has been installed directly on the die. White diodes illuminate the coating gap from the backside, and pattern formation can be observed directly in the coating gap of 220 μm height between the die and the substrate. These additional experiments have clearly demonstrated that the parallel stripes appear directly at the die and are neither due to a later rearrangement of the liquid on the substrate nor do they result from solvent evaporation. A snapshot of the die during the coating process is provided in Fig. 11(b).

To analytically assess the role of evaporation and potential Marangoni flows during the coating process, we consider the Marangoni number $\mathrm{Ma} = -\frac{\partial \sigma}{\partial T} \frac{H \Delta T}{\eta \alpha}$, where ΔT is the vertical temperature difference in the coated layer of characteristic height H, and $\alpha = 0.08\,\mathrm{mm^2/s}$ is the thermal diffusivity of ethanol.[69] To estimate Ma, we assume that the dependence of the surface tension on the temperature is of order $-0.3\,\mathrm{mN/(m\,K)}$ (similar to aqueous solutions[70]) and that the evaporation-induced temperature difference is $\Delta T = 0.25\,\mathrm{K}$ (as, e.g., in Ref. 71). Further, we use a characteristic film height of $H = 20\,\mu$m. Then, the Marangoni number is in the range $\mathrm{Ma} \in [0.02, 0.63]$ for viscosities $\eta \in [10\,\mathrm{cP}, 400\,\mathrm{cP}]$, supporting our assumption that thermal Marangoni effects are insignificant during the coating process. Moreover, solutal Marangoni flows cannot explain the pattern formation, as the surface tension depends weakly on the PVP concentration and, here, evaporation of the solvent, i.e., an
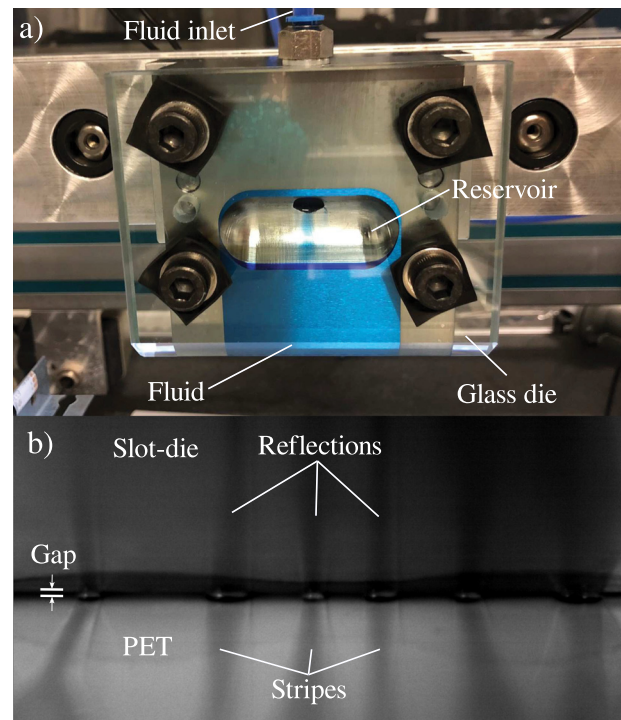

FIG. 11. (a) Image of the slot-die system with glass front plate used to control the coating liquid homogeneity in the die. (b) Image made during the coating with a CCD camera installed on the slot-die: The coating gap is in the middle; the stripes on PET (also seen in the reflection on the slot-die) are formed immediately at the die.

accumulation of PVP at the surface, would actually induce a stabilizing flow. However, on a larger timescale, the coated layers and structures slowly dry. This can indeed result in an additional low-amplitude small-scale pattern. Due to the rather weak Marangoni flows,[72] in our system these drying patterns only appear several minutes after the coating process has ended. The resulting secondary pattern is of a different (convective) nature than the primary pattern discussed in our work. A deeper analysis is beyond our present scope.

Further, it has been checked that the parallel stripes are not already produced by flow instabilities within the die before the liquid leaves the slot. To do so, the metallic front plate of the die has been substituted by a transparent glass plate, see Fig. 11(a). Additional experiments (not shown here) have confirmed (i) that the replacement of metal by glass does not noticeably change the observed parameter ranges and the transition scenarios, and (ii) that the flow inside the die is always homogeneous (also no air bubbles were observed in the slot channel).

In both, experiment and simulations, the patterns were susceptible to defects. To acquire an understanding of the topology of defects and the stability of the patterns to perturbations, the experimental setup needs to be extended to allow for longer coated distances.

In conclusion, focusing on parameter regimes outside the coating window, we have achieved some insight into the formation of patterns in slot-die coating and their sequence of occurrence.

Changing several principal parameters, we have revealed transitions from homogeneous coating inside the coating window to various stripe patterns, mixed and irregular patterns. Furthermore, we have established a relatively simple thin-film model for the coating hydrodynamics at the meniscus. In this way, we have been able to model an identical set of patterns and pertinent transitions. A discussion of agreements and disagreements between our experimental and theoretical approaches has let us outline possible steps for further research.

AUTHOR DECLARATIONS

Conflict of Interest

The authors have no conflicts to disclose.

Author Contributions

Maren Kasischke: Investigation (equal); Visualization (equal); Writing – original draft (equal); Writing – review & editing (equal). **Simon Hartmann:** Investigation (equal); Software (equal); Visualization (equal); Writing – original draft (equal); Writing – review & editing (equal). **Kevin Niermann:** Investigation (equal); Visualization (equal). **Marco Smarra:** Investigation (equal); Visualization (equal). **Denis Kostyrin:** Investigation (equal); Visualization (equal). **Uwe Thiele:** Funding acquisition (equal); Supervision (equal); Writing – review & editing (equal). **Evgeny L. Gurevich:** Funding acquisition (equal); Project administration (equal); Supervision (equal); Writing – original draft (equal); Writing – review & editing (equal).

DATA AVAILABILITY

The data that support the findings of this study are available from the corresponding author upon reasonable request.
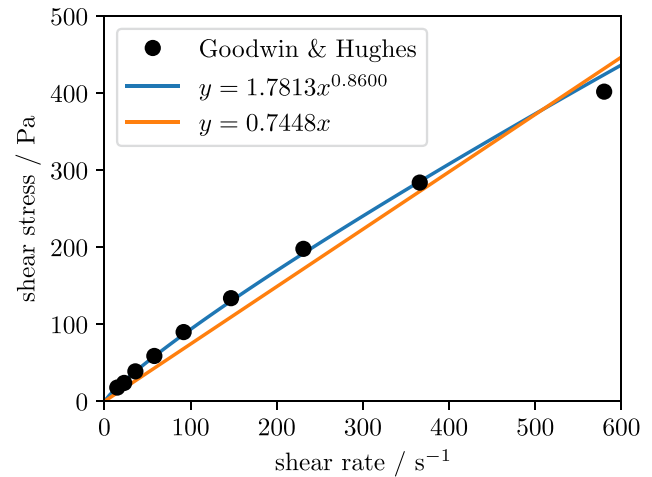

FIG. 12. Shear stress vs shear rate for a 12% PVP–ethanol solution according to Goodwin and Hughes[51] (black dots), their power law fit (blue line), and a linear fit (orange line). As the linear fit deviates only weakly from the data, the liquid can be considered as a Newtonian liquid.

APPENDIX A: NEWTONIAN BEHAVIOR OF THE PVP–ETHANOL SOLUTION

The employed coating liquid, a 5%–9% PVP–ethanol mixture, is considered to be Newtonian throughout this work. In Fig. 12, we reproduce the shear stress measurements for a 12% PVP solution published by Goodwin and Hughes[51] and show additional fits to a linear law and a power law. The shear rate ranges from 0 to $600\,\mathrm{s^{-1}}$ and the power-law behavior is rather weak. While the power-law fit (blue line) indicates a power of 0.86, a linear (i.e., Newtonian) fit shows only a small deviation from their curve (orange line).

APPENDIX B: EFFECTS OF SOLVENT EVAPORATION

Evaporation of the solvent can also induce Marangoni flows that cause pattern formation to occur in a uniform film of a solution or suspension[73–75] or, indeed, a film of simple volatile liquid.[72,76]
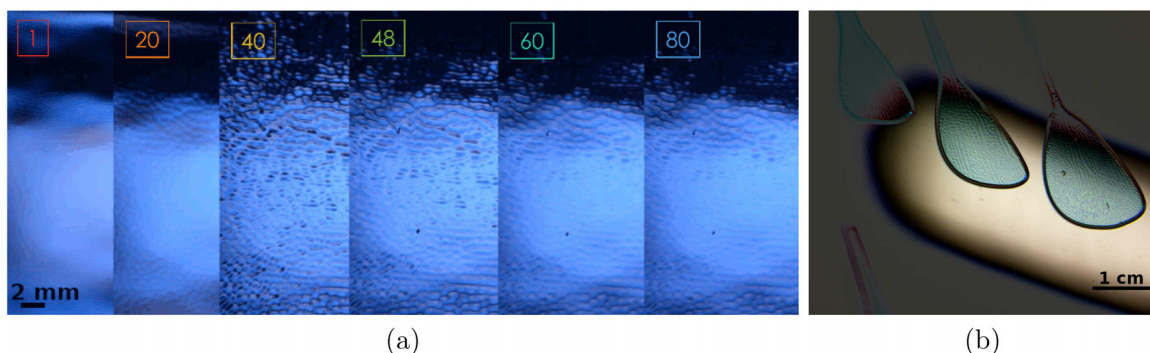

FIG. 13. (a) Drying pattern in a homogeneous layer recorded at different times with a frame rate of three frames per minute starting immediately after the coating process, and the number in the box indicates the frame number. The scale bar shown in the first frame applies to all frames. (b) A coating pattern consisting of drops with a barely visible small-scale pattern that modulates the drop's plateau height thickness. The weak modulation results from solvent evaporation well after the initial coating and is captured several days after the coating. The bright spot is the reflection of the illumination source needed to make the small-scale pattern visible.

To investigate whether and at what timescale such an effect may occur in our system, we dry homogeneously coated layers of PVP solution at room temperature. Three frames per minute are captured with a conventional photo camera for several minutes starting immediately after the end of the coating process, see Fig. 13(a). After approximately 7–10 min, a barely visible small-scale pattern becomes visible. Due to the small amplitude of the resulting height modulations of the layer, the resulting pattern can only be seen at acute viewing and illumination angles. The observed small amplitude pattern can consist of parallel stripes, maze-like structures, or localized structures with characteristic length scales of approximately 1 mm. These pattern types well correspond to the ones expected for such an evaporation-driven small-scale instability.[72,77]

Such evaporation-driven instabilities also affect the coating-produced structures reported in Sec. III. However, they do not occur on the timescale of the coating process but on a much larger timescale. Then, the additional instability slightly modulates the thickness profile of the coated structures without changing the coating patterns. As an example, we show in Fig. 13(b) one irregular pattern at high viewing and illumination. Although pattern formation due to solvent evaporation is itself an interesting research topic, here, we only confirm that the evaporative instability does not affect the large-scale coating pattern, i.e., the width and arrangement of the coated stripes remain unchanged. A deeper investigation is out of our present scope.

REFERENCES

[1]J. Chang, C. Chi, J. Zhang, and J. Wu, "Controlled growth of large-area high-performance small-molecule organic single-crystalline transistors by slot-die coating using a mixed solvent system," Adv. Mater. **25**, 6442–6447 (2013).

[2]A. Sandström, H. F. Dam, F. C. Krebs, and L. Edman, "Ambient fabrication of flexible and large-area organic light-emitting devices using slot-die coating," Nat. Commun. **3**, 1002 (2012).

[3]G. R. Cagnani, G. Ibáñez-Redín, B. Tirich, D. Gonçalves, D. T. Balogh, and O. N. Oliveira, "Fully-printed electrochemical sensors made with flexible screen-printed electrodes modified by roll-to-roll slot-die coating," Biosens. Bioelectron. **165**, 112428 (2020).

[4]J. Sharma, X. Lyu, T. Reshetenko, G. Polizos, K. Livingston, J. Li, D. L. Wood, and A. Serov, "Catalyst layer formulations for slot-die coating of PEM fuel cell electrodes," Int. J. Hydrogen Energy **47**, 35838–35850 (2022).

[5]P. Liu, D. Yang, B. Li, C. Zhang, and P. Ming, "Recent progress of catalyst ink for roll-to-roll manufacturing paired with slot die coating for proton exchange membrane fuel cells," Int. J. Hydrogen Energy **48**, 19666 (2023).

[6]F. C. Krebs, "Polymer solar cell modules prepared using roll-to-roll methods: Knife-over-edge coating, slot-die coating and screen printing," Sol. Energy Mater. Sol. Cells **93**, 465–475 (2009).

[7]F. Jakubka, M. Heyder, J. Kaschta, F. Machui, and C. Brabec, "Determining the coating speed limitations for organic photovoltaic inks," Sol. Energy Mater. Sol. Cells **109**, 120–125 (2013).

[8]R. Patidar, D. Burkitt, K. Hooper, D. Richards, and T. Watson, "Slot-die coating of perovskite solar cells: An overview," Mater. Today Commun. **22**, 100808 (2020).

[9]H. Zhao, H. B. Naveed, B. Lin, X. Zhou, J. Yuan, K. Zhou, H. Wu, R. Guo, M. A. Scheel, A. Chumakov, S. V. Roth, Z. Tang, P. Müller-Buschbaum, and W. Ma, "Hot hydrocarbon-solvent slot-die coating enables high-efficiency organic solar cells with temperature-dependent aggregation behavior," Adv. Mater. **32**, 2002302 (2020).

[10]Z. Yang, W. Zhang, S. Wu, H. Zhu, Z. Liu, Z. Liu, Z. Jiang, R. Chen, J. Zhou, Q. Lu, Z. Xiao, L. Shi, H. Chen, L. K. Ono, S. Zhang, Y. Zhang, Y. Qi, L. Han, and W. Chen, "Slot-die coating large-area formamidinium-cesium perovskite film for efficient and stable parallel solar module," Sci. Adv. **7**, eabg3749 (2021).

[11]M. S. Carvalho and H. S. Kheshgi, "Low-flow limit in slot coating: Theory and experiments," AIChE J. **46**, 1907–1917 (2000).

[12]E. B. Gutoff and E. D. Cohen, *Coating and Drying Defects: Troubleshooting Operating Problems*, 2nd ed. (Wiley, Hoboken, NJ, 2006).

[13]X. Y. Ding, J. H. Liu, and T. A. L. Harris, "A review of the operating limits in slot die coating processes," AIChE J. **62**, 2508–2524 (2016).

[14]K. Bhamidipati, S. Didari, and T. A. L. Harris, "Experimental study on air entrainment in slot die coating of high-viscosity, shear-thinning fluids," Chem. Eng. Sci. **80**, 195–204 (2012).

[15]S. M. Raupp, M. Schmitt, A.-L. Walz, R. Diehm, H. Hummel, P. Scharfer, and W. Schabel, "Slot die stripe coating of low viscous fluids," J. Coat. Technol. Res. **15**, 899 (2018).

[16]U. Thiele, "Patterned deposition at moving contact line," Adv. Colloid Interface Sci. **206**, 399–413 (2014).

[17]R. G. Larson, "Transport and deposition patterns in drying sessile droplets," AIChE J. **60**, 1538–1571 (2014).

[18]H. Bodiguel and J. Leng, "Imaging the drying of a colloidal suspension," Soft Matter **6**, 5451–5460 (2010).

[19]F. Doumenc and B. Guerrier, "Self-patterning induced by a solutal Marangoni effect in a receding drying meniscus," Europhys. Lett. **103**, 14001 (2013).

[20]G. Berteloot, A. Daerr, F. Lequeux, and L. Limat, "Dip coating with colloids and evaporation," Chem. Eng. Process. **68**, 69–73 (2013).

[21]M. Gleiche, L. F. Chi, and H. Fuchs, "Nanoscopic channel lattices with controlled anisotropic wetting," Nature **403**, 173–175 (2000).

[22]L. Q. Li, M. H. Köpf, S. V. Gurevich, R. Friedrich, and L. F. Chi, "Structure formation by dynamic self-assembly," Small **8**, 488–503 (2012).

[23]M. H. Köpf and U. Thiele, "Emergence of the bifurcation structure of a Langmuir-Blodgett transfer model," Nonlinearity **27**, 2711–2734 (2014).

[24]W. Han and Z. Lin, "Learning from 'Coffee Rings': Ordered structures enabled by controlled evaporative self-assembly," Angew. Chem., Int. Ed. **51**, 1534–1546 (2012).

[25]L. Fraštia, A. J. Archer, and U. Thiele, "Modelling the formation of structured deposits at receding contact lines of evaporating solutions and suspensions," Soft Matter **8**, 11363–11386 (2012).

[26]X. Y. Yang, Z. C. Jiang, P. H. Lyu, Z. Y. Ding, and X. K. Man, "Deposition pattern of drying droplets," Commun. Theor. Phys. **73**, 047601 (2021).

[27]S. Lee, A. M. Tiara, G. Cho, and J. Lee, "Control of the drying patterns for complex colloidal solutions and their applications," Nanomaterials **12**, 2600 (2022).

[28]P. Kubis, N. Li, T. Stubhan, F. Machui, G. J. Matt, M. M. Voigt, and C. J. Brabec, "Patterning of organic photovoltaic modules by ultrafast laser," Prog. Photovoltaics **23**, 238–246 (2015).

[29]S. Lenhert, L. Zhang, J. Mueller, H. P. Wiesmann, G. Erker, H. Fuchs, and L. F. Chi, "Self-organized complex patterning: Langmuir-Blodgett lithography," Adv. Mater. **16**, 619–624 (2004).

[30]D. Mampallil and H. B. Eral, "A review on suppression and utilization of the coffee-ring effect," Adv. Colloid Interface Sci. **252**, 38–54 (2018).

[31]A. Bournigault-Nuquet, S. Couderc, J. Bibette, and J. Baudry, "Patterning of a drying emulsion film," Langmuir **37**, 8924–8928 (2021).

[32]J. Nam and M. S. Carvalho, "Flow visualization and operating limits of tensioned-web-over slot die coating process," Chem. Eng. Process.: Process Intensif. **50**, 471–477 (2011).

[33]C.-F. Lin, D. S. Hill Wong, T.-J. Liu, and P.-Y. Wu, "Operating windows of slot die coating: Comparison of theoretical predictions with experimental observations," Adv. Polym. Technol. **29**, 31–44 (2010).

[34]C. F. Lin, B. K. Wang, S. H. Lo, D. S. H. Wong, T. J. Liu, and C. Tiu, "Operating windows of stripe coating," Asia-Pac. J. Chem. Eng. **9**, 134–145 (2014).

[35]S. Khandavalli and J. P. Rothstein, "The effect of shear-thickening on the stability of slot-die coating," AIChE J. **62**, 4536–4547 (2016).

[36]M. Schmitt, M. Baunach, L. Wengeler, K. Peters, P. Junges, P. Scharfer, and W. Schabel, "Slot-die processing of lithium-ion battery electrodes-coating window characterization," Chem. Eng. Process. **68**, 32–37 (2013).

[37]O. J. Romero, W. J. Suszynski, L. E. Scriven, and M. S. Carvalho, "Low-flow limit in slot coating of dilute solutions of high molecular weight polymer," J. Non-Newtonian Fluid Mech. **118**, 137–156 (2004).

[38]R. Malakhov, K. Tjiptowidjojo, and P. R. Schunk, "Mechanics of the low-flow limit in slot-die coating with no vacuum," AIChE J. **65**, e16593 (2019).

[39] P. Gao, L. Li, J. J. Feng, H. Ding, and X.-Y. Lu, "Film deposition and transition on a partially wetting plate in dip coating," J. Fluid Mech. **791**, 358–383 (2016).

[40] W. Tewes, M. Wilczek, S. V. Gurevich, and U. Thiele, "Self-organised dip-coating patterns of simple, partially wetting, nonvolatile liquids," Phys. Rev. Fluids **4**, 123903 (2019).

[41] H. Kang, J. Park, and K. Shin, "Statistical analysis for the manufacturing of multi-strip patterns by roll-to-roll single slot-die systems," Rob. Comput. Integr. Manuf. **30**, 363–368 (2014).

[42] M. A. Jabal, A. Egbaria, A. Zigelman, U. Thiele, and O. Manor, "Connecting monotonic and oscillatory motions of the meniscus of a volatile polymer solution to the transport of polymer coils and deposit morphology," Langmuir **34**, 11784–11794 (2018).

[43] M. Pichumani, P. Bagheri, K. M. Poduska, W. Gonzalez-Vinas, and A. Yethiraj, "Dynamics, crystallization and structures in colloid spin coating," Soft Matter **9**, 3220–3229 (2013).

[44] M. Maleki, M. Reyssat, F. Restagno, D. Quéré, and C. Clanet, "Landau-Levich menisci," J. Colloid Interface Sci. **354**, 359–363 (2011).

[45] M. Dey, F. Doumenc, and B. Guerrier, "Numerical simulation of dip-coating in the evaporative regime," Eur. Phys. J. E **39**, 19 (2016).

[46] M. H. Köpf, S. V. Gurevich, R. Friedrich, and U. Thiele, "Substrate-mediated pattern formation in monolayer transfer: A reduced model," New J. Phys. **14**, 023016 (2012).

[47] P.-M. T. Ly, K. D. J. Mitas, U. Thiele, and S. V. Gurevich, "Two-dimensional patterns in dip coating—First steps on the continuation path," Physica D **409**, 132485 (2020).

[48] P.-M. T. Ly, U. Thiele, L. Chi, and S. V. Gurevich, "Effects of time-periodic forcing in a Cahn-Hilliard model for Langmuir-Blodgett transfer," Phys. Rev. E **99**, 062212 (2019).

[49] S. Engelnkemper, S. V. Gurevich, H. Uecker, D. Wetzel, and U. Thiele, "Continuation for thin film hydrodynamics and related scalar problems," in *Computational Modeling of Bifurcations and Instabilities in Fluid Mechanics*, Computational Methods in Applied Sciences, Vol. 50, edited by A. Gelfgat (Springer, Cham, 2019), pp. 459–501.

[50] O. Kim and J. Nam, "Confinement effects in dip coating," J. Fluid Mech. **827**, 1–30 (2017).

[51] J. W. Goodwin and R. W. Hughes, *Rheology for Chemists: An Introduction* (The Royal Society of Chemistry, Cambridge, 2000).

[52] C. A. Schneider, W. S. Rasband, and K. W. Eliceiri, "NIH Image to ImageJ: 25 years of image analysis," Nat. Methods **9**, 671 (2012).

[53] M. Taghizadeh and S. S. Amiri, "Experimental measurements and modeling of solvent activity and surface tension of binary mixtures of polyvinylpyrrolidone in water and ethanol," J. Serb. Chem. Soc. **82**, 427–435 (2017).

[54] O. J. Romero, L. E. Scriven, and M. S. Carvalho, "Slot coating of mildly viscoelastic liquids," J. Non-Newtonian Fluid Mech. **138**, 63–75 (2006).

[55] D. Maza and M. S. Carvalho, "Transient response of two-layer slot coating flows to periodic disturbances," AIChE J. **61**, 1699–1707 (2015).

[56] A. Oron, S. H. Davis, and S. G. Bankoff, "Long-scale evolution of thin liquid films," Rev. Mod. Phys. **69**, 931–980 (1997).

[57] U. Thiele, "Structure formation in thin liquid films," in *Thin Films of Soft Matter*, edited by S. Kalliadasis and U. Thiele (Springer, Vienna, 2007), pp. 25–93.

[58] R. V. Craster and O. K. Matar, "Dynamics and stability of thin liquid films," Rev. Mod. Phys. **81**, 1131–1198 (2009).

[59] J. H. Snoeijer, B. Andreotti, G. Delon, and M. Fermigier, "Relaxation of a dewetting contact line. Part 1. A full-scale hydrodynamic calculation," J. Fluid Mech. **579**, 63–83 (2007).

[60] J. Ziegler, J. H. Snoeijer, and J. Eggers, "Film transitions of receding contact lines," Eur. Phys. J.: Spec. Top. **166**, 177–180 (2009).

[61] M. Galvagno, D. Tseluiko, H. Lopez, and U. Thiele, "Continuous and discontinuous dynamic unbinding transitions in drawn film flow," Phys. Rev. Lett. **112**, 137803 (2014).

[62] P.-G. De Gennes, "Wetting: Statics and dynamics," Rev. Mod. Phys. **57**, 827 (1985).

[63] B. V. Derjaguin, N. V. Churaev, V. M. Muller, and V. I. Kisin, *Surface Forces* (Springer, New York, 1987).

[64] U. Thiele, "Thin film evolution equations from (evaporating) dewetting liquid layers to epitaxial growth," J. Phys.: Condens. Matter **22**, 084019 (2010).

[65] N. V. Churaev, "Contact angles and surface forces," Adv. Colloid Interface Sci. **58**, 87–118 (1995).

[66] M. Heil and A. L. Hazel, "Oomph-lib—An object-oriented multi-physics finite-element library," in *Fluid-Structure Interaction: Modelling, Simulation, Optimisation*, edited by H.-J. Bungartz and M. Schäfer (Springer, Berlin/Heidelberg, 2006), pp. 19–49.

[67] A. L. Yarin, *Free Liquid Jets and Films: Hydrodynamics and Rheology*, Interaction of Mechanics and Mathematics Series (Longman Scientific & Technical, New York, 1993).

[68] A. Kolbasov, S. Sinha-Ray, A. Joijode, M. A. Hassan, D. Brown, B. Maze, B. Pourdeyhimi, and A. L. Yarin, "Industrial-scale solution blowing of soy protein nanofibers," Ind. Eng. Chem. Res. **55**, 323–333 (2016).

[69] D. R. Lide, *CRC Handbook of Chemistry and Physics* (CRC Press, Boca Raton, FL, 2004), Vol. 85.

[70] J. Águila-Hernández, A. Trejo, and B. E. García-Flores, "Volumetric and surface tension behavior of aqueous solutions of polyvinylpyrrolidone in the range (288 to 303) K," J. Chem. Eng. Data **56**, 2371–2378 (2011).

[71] M. Tönsmann, P. Scharfer, and W. Schabel, "Critical solutal Marangoni number correlation for short-scale convective instabilities in drying poly(vinyl acetate)-methanol thin films," Polymers **13**, 2955 (2021).

[72] F. Chauvet, S. Dehaeck, and P. Colinet, "Threshold of Bénard-Marangoni instability in drying liquid films," Europhys. Lett. **99**, 34001 (2012).

[73] M. Maillard, L. Motte, A. T. Ngo, and M. P. Pileni, "Rings and hexagons made of nanocrystals: A Marangoni effect," J. Phys. Chem. B **104**, 11871–11877 (2000).

[74] E. Bormashenko, R. Pogreb, A. Musin, O. Stanevsky, Y. Bormashenko, G. Whyman, O. Gendelman, and Z. Barkay, "Self-assembly in evaporated polymer solutions: Influence of the solution concentration," J. Colloid Interface Sci. **297**, 534–540 (2006).

[75] H. Ma and J. Hao, "Ordered patterns and structures via interfacial self-assembly: Superlattices, honeycomb structures and coffee rings," Chem. Soc. Rev. **40**, 5457–5471 (2011).

[76] B. Haut and P. Colinet, "Surface-tension-driven instabilities of a pure liquid layer evaporating into an inert gas," J. Colloid Interface Sci. **285**, 296–305 (2005).

[77] M. Bestehorn and D. Merkt, "Regular surface patterns on Rayleigh-Taylor unstable evaporating films heated from below," Phys. Rev. Lett. **97**, 127802 (2006).

25 July 2023 13:26:17